Ovonic Threshold Switch chalcogenides: connecting first-principles electronic structure to selector device parameters

Sergiu Clima,[1*] Taras Ravsher,[1,2] Daniele Garbin,[1] Robin Degraeve,[1] Andrea Fantini,[1] Romain Delhougne,[1] Gouri Sankar Kar,[1] Geoffrey Pourtois,[1,3]
[1] imec, B-3001 Leuven, Belgium, [2]KU Leuven, B-3000 Leuven, Belgium
[3] University of Antwerp, B-2610 Antwerp, Belgium
* sergiu.clima@imec.be

Abstract — Chalcogenides are attractive materials for microelectronics applications due to their ability to change physical, optical and electrical properties under applied electric stimulus. One of the most recent interests in chalcogenides is their use to enable the development of a two-terminal selector device, which is a fast, volatile, resistance switching device. The electrical signature of Ovonic Threshold Switching (OTS) chalcogenide materials is well suited for such applications. While there are numerous known OTS materials, most of them contain toxic elements. There is hence a need to find environment-friendly OTS materials. For this to happen, we strive to predict electrical device parameters only from atomistic first-principles simulations of the chalcogenide materials, as this can be a faster and less expensive route to screen the performances of chalcogenides candidates. By mapping the experimentally measured set of electrical OTS materials into atomistic models and computing their electronic properties, we were able to identify correlations between computed properties such as the theoretical trap/mobility gaps, the local atomic coordination environments of the elements adopted in the material and the experimentally-measured first-fire/ threshold/ hold voltages, hold / leakage currents or extracted trap density. These findings can guide in identifying OTS material with predefined electronic properties, tailored to the requirements of specific microelectronics applications with only first-principles simulations.

KEYWORDS: OTS, Ovonic switching, chalcogenide, selector, first principles.

I. INTRODUCTION

Chalcogenide materials are currently widely used in the industry as optical [1-4] or electrical memory storage [5-9]. These materials' ability to reversibly crystallize or amorphize, depending on the applied temperature profile, and therefore showing contrasting properties, made certain chalcogenides like $Ge_xSb_yTe_z$ family the pinnacle of the CD/ DVD/ Blue-ray era [1-3,10-12]. For optical data storage, the information is stored using a modulation of the reflectivity index by inducing a controlled local heating of the material. With the rise of the flash era [13-15], the microelectronics industry switched to solid-state storage media. To bridge the performance gap between Dynamic Random Access Memories (DRAM) and the flash-based Solid State Drives (SSD), a new Storage-Class-Memory (SCM) has been proposed [16,17]. SCM fits in well the phase-change materials: their cycling capability is few orders of magnitude higher than that of the flash memories and their state retention is respectably longer than that of the DRAM. For solid-state applications, the contrasting property is the difference in conductivity that two states of the material display. Instead of a change in bulk reflectivity, the chalcogenides adopt a resistance switching mechanism as reported in resistive type memories [5-7,18,19]. The temperature profile is induced by the Joule-heating effect of the current passing through the device and the special cell design for appropriate thermal heating/ dissipation. Dealing with large memory device arrays becomes prone to reading errors, when half-selected word/bit-lines contact memory cells in low-resistance state: the "sneak-path" current can exceed the current on the selected high-resistance-state cell (Fig. 1a). This requires the use of an access device, such as a selector [20].

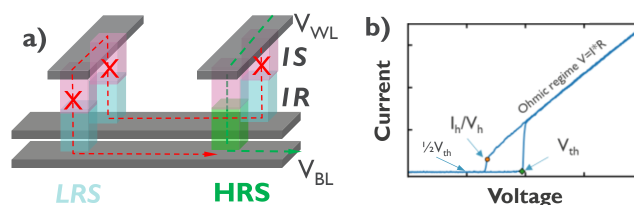

Fig. 1 a) Schematic role of the SELECTOR device in series with resistive memory element (1S1R) – cut the parasitic leakage on half-biased low-resistance-state memory cells, while allowing the correct reading of a high-resistance-state memory cell. b) I-V characteristics of the OTS materials, showing the definitions of the threshold/hold voltages and currents.

Ongoing efforts to develop two-terminal selector devices are directed towards suppressing the sneak-path leakage currents. Ovonic Threshold Switching (OTS) chalcogenide materials seem very promising in that respect, since these materials display volatile resistive switching characteristics: at half of threshold voltage, the leakage current through the material is orders of magnitude lower (Fig. 1b) [20-24]. The volatile resistive switching has been coined by the name of the researcher who discovered the effect: Ovonic (Ovshinsky) Threshold Switching[23]. Aside from selector device, the OTS materials can also be used as stand-alone self-rectified memory device [25].

Many available OTS materials are S- [26], Se-[21] or Te-based [24,27], many contain As to slow down the crystallization [7,28]. The recent health and environmental trends impose a reduction of the usage of hazardous / toxic materials [29,30], hence there is a need to find new OTS materials that use less polluting or hazardous elements. Screening for new materials among thousands or millions of possible compositions seems impossible. Theoretical simulations screening, however, is a much more viable alternative. For this approach to work,

This document is the Accepted Manuscript version of a Published Work that appeared in final form in ACS Applied Electronics Materials, © 2022 American Chemical Society after peer review and technical editing by the publisher. To access the final edited and published work see https://doi.org/10.1021/acsaelm.2c01458

researchers need to know which theoretical parameters are important to screen for, when searching for a material with well-defined experimental parameters. Therefore, understanding the OTS mechanism and the correlations between material properties and device parameters is of utmost importance.

The working principle of the OTS mechanism is still debated: some researchers model it with purely electronic effects [6,23,31-34], while others also consider local atomic relaxation to be of importance [7,35-40]. Recent first-principles efforts suggest that both electronic excitations and/or polaron relaxation can change the electronic conductivity on the local atomic scale, therefore highlighting the importance of both electronic and ionic relaxation in the disordered atomic systems [7,39,40]. Even if the many existing theories complement each-other, the OTS mechanism understanding is still far from being complete. In our effort to contribute with additional insights, we performed data analysis to correlate the experimental measurements with theoretical predictions. For this, we investigated the same series of OTS materials both from ab-initio and experimental point of view. These correlations allow us to map the expected experimental device parameters directly from the theoretically-computed electronic properties of a material. It enables the screening for and the selection of a hypothetical material for building a technologically-relevant device with predefined electrical specifications using only first-principles simulations [41].

Following the order of the operation of an OTS device (Fig. 1b), we start with the description of the first-fire and threshold voltages that put the OTS in the Ohmic regime (ON), then continue towards ramping-down the voltage to describe the hold current/ voltage correlations, after which the device switches OFF. Finally, we investigate material parameters and structural morphologies to correlate them with electrical measurements and conclude.

II. Methodology

A. DFT computations

Ab-initio Density Functional Theory (DFT) simulations were performed in CP2K[42] by describing the core electrons with GTH pseudopotentials,[43] and the valence electrons by a mix of double-zeta-valence-polarization (DZVP) localized Gaussian basis sets and planewaves with a cutoff of 500 Ry and a relative cutoff of 40 Ry for the real space integration grid. The planewaves were integrated on four sub-grids to calculate the charge density. A Generalized Gradient Approximation (PBE)[44] or a hybrid (HSE06)[45] functional was employed to describe the exchange and correlation of the electrons. The Brillouin zone was sampled with Γ-point only for all models.

Amorphous model generation protocol consists in a decorate-and-relax procedure,[46,47] by randomly placing the anionic species at equidistant locations in a periodic box that would correspond to a 10-15% decrease of the material density. Subsequently, the cationic species are distributed around the anions, respecting the corresponding coordination numbers and bond distances. A fast volume relaxation is followed by a more rigorous full atomic relaxation, where the atomic forces were relaxed below 1E-4 Ha/bohr, whereas the cell parameters were relaxed until the pressure dropped below 100 bar. The resulting amorphous models generated with such a procedure were found to be similar to the ones generated with a melt-and-quench method in ab-initio molecular dynamics.[47]

For the *ab-initio* mobility gap estimation, a hybrid exchange-correlation functional (HSE06) was used in combination with the Auxiliary Density Matrix Method (ADMM) to accurately quantify the electronic structure.[48] We used the inverse participation ratio (IPR) to identify the mobility edges of the atomic models.[49] As valence edge, we take the highest occupied state with an IPR value equal to the median of the distribution in the valence band. Whereas for the conduction edge - the lowest empty state with the same criterion for the IPR value. The mobility gap is taken as the energy difference between the valence and conduction edges. The electron/hole trap states are extracted from the DOS data and represent the deepest levels with respect to conduction band (for electrons) or valence band (for holes), respectively. To ensure a representative estimation of the electronic / atomic properties, we performed statistics over 10 different amorphous models that contain 300 atoms and lateral size around 2nm, which is larger than the minimum of 1.5nm of the amorphous model that is required to see localization in the electronic states of the amorphous chalcogenides.[22,39]

B. Experimental details

To measure the experimental parameters, a set of devices with different OTS material compositions was fabricated. The device consisted of an OTS film sandwiched between the top and bottom TiN electrodes. The bottom electrode was etched into a pillar with critical dimension (CD) defined down to 55nm. A 20 nm thick OTS film together with TE metal was deposited on top of BE, resulting in a mushroom-type cell structure. Various OTS compositions were tested, including ternary and quaternary (Si)-Ge-As-Te and (Si)-Ge-As-Se material systems, deposited by means of physical vapor deposition (PVD) technique [50]. The atomic compositions were investigated by means of PIXE (Particle-Induced X-ray Emission), XRF (X-Ray Fluorescence) and RBS (Rutherford Backscattering Spectroscopy).

The devices were electrically characterized using a series of triangular ac pulses with a rise time of t_{rise}=10 μs and an amplitude of 9V or 7V for the first-fire and consequent 10 switching cycles, respectively. From these measurements first-fire (V_{FF}) and threshold voltage (V_{th}) values were extracted for a set of 10 dies to extract the mean and standard deviations. Additionally, sub-threshold leakage was extracted from a dc measurement. Structures with nominal CD=65 nm were used for the ac characterization. An integrated series resistor was used to limit the current in the ON-state (R_s~10kΩ, unless specified otherwise). Holding voltage (V_h) is the R_s-corrected voltage across OTS layer. Additionally, the number of quenched defects in the OTS conduction cluster (N_d) was estimated from the statistical properties of V_{th} distribution.[51]

III. Results and Discussion

In a first stage, we developed [50] various OTS selector devices and characterized their performance parameters, like first-fire (V_{ff}), threshold (V_{th}) and hold voltages (V_h) and currents (I_h). We collected electrical data for a set of nine GeAsSe,

SiGeAsTe, and SiGeAsSe OTS materials with various compositions, as listed in Table 1.

Table 1. Experimental sample compositions, mean number of valence electrons per atom (#e) and mean coordination numbers (MCN) for the investigated materials.

id	Material	Si%	Ge%	As%	Te(Se)%	#e	MCN
1	SiGeAsTe-A	16	16	28	40	5.08	2.92
2	SiGeAsTe-B	7	20	30	43	5.16	2.84
3	SiGeAsTe-C	15	8	46	31	5.08	2.92
4	SiGeAsTe-D	8	21	42	29	5.00	3.00
5	GeAsSe-A	0	18	34	48	5.30	2.70
6	GeAsSe-B	0	26	32	42	5.16	2.84
7	GeAsSe-C	0	37	28	35	4.98	3.02
8	SiGeAsSe-A	10	9	34	47	5.28	2.72
9	SiGeAsSe-B	9	16	31	44	5.19	2.81

Next, we generated 10 different atomistic models for each composition to do statistical averaging of the computed properties. For each model, we predicted the electronic properties from first-principles: Born effective charges (Z*) [52], electron/hole trap depths (E_t/E_h) in the gap and the mobility gaps (E_μ) (Fig. 2).

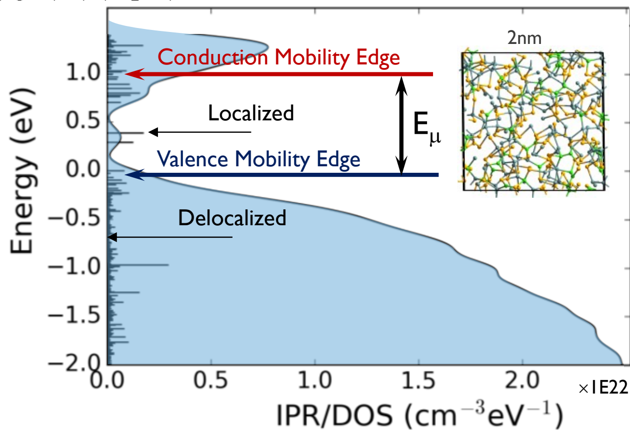

Fig. 2. Density of States (DOS) and Inverse Participation Ratio (IPR –horizontal bars) computed for relaxed atomistic models are used to identify the mobility gap (E_μ), electron/hole trap depth and the trap gap (ΔE_t).

Also, the atomic structure coordination environments around each atom were extracted.[53,54] For all above-mentioned properties, the median values were correlated with the electrical measurement data (which are also median values over 11 devices across the wafer), as presented below.

A. OTS materials characteristics

Valence electrons (#e): The mean valence electrons of the OTS materials should be in the range of 5 valence electrons per atom for the OTS mechanism to be active [55,56]. This can be rationalized with a simple bond formation between 2 elements: if we have an anion A (for ex: Se,Te) with s^2p^4 and a cation B (for ex: Ge) with s^2p^2 electronic configuration in the top valence states, the total number of electrons in the AB (GeSe or GeTe) compound is enough to pair-up and form 3 bonds (p^6), leaving s^2 pairs of electrons non-bonding (if we disregard the hybridization, which is reasonable, considering that low hybridization elements are desired for OTS [57]) and other 3 empty anti-bonding p^{*0} orbitals. This configuration for the two elements would average 5 valence electrons/atom and for a perfect crystal would result in completely filled valence and empty conduction states with a semiconducting/insulating electronic bandgap. With the disorder of the amorphous state of the material, however, the local variations of the stoichiometry/ number of electrons/ orbitals results in Anderson-localized states, instead of bands (crystalline counterparts) [58,59]. The most shallow in energy valence states that have the delocalization length larger than the device size will play the role of the valence mobility edge. Higher in energy states localized inside the device will become tail-states if close in energy to the mobility edge, or gap-states if energetically deeper into the electronic gap. The same applies symmetrically for the conduction side (Fig. 2). It is these tail- and gap-states that OTS mechanism relies upon. The average valence electrons number varies between 5 and 5.3 for the 9 OTS material compositions we investigated in this study (Table 1). A weak but positive correlation of the mean valence electrons with the threshold (V_{th}) / holding (V_h) voltages of the 9 compositions was identified (Supplementary Fig S1), hinting to the fact that additional (to the average 5) electrons would fill-in the empty bonding orbitals in the valence tail-states, energetically stabilizing /deactivating them.

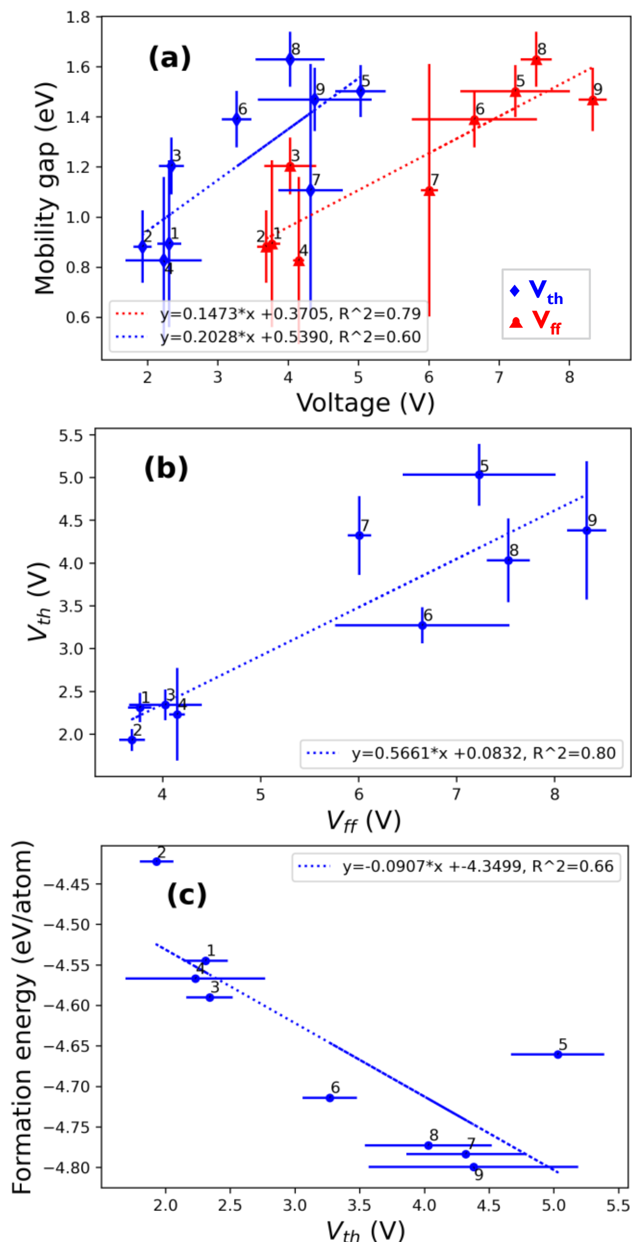

Fig. 3 (a) Experimental threshold (V_{th}) and first-fire voltage (V_{ff}) correlation to the DFT predicted mobility gap. (b) Positive correlation of the experimental V_{ff} and V_{th}. Error bars show the standard deviation from 10 samples. (c) Negative correlation between materials formation energies and threshold voltages. Data points labeled with material id from Table 1.

Mean coordination numbers (MCN): maintaining a topologically-constrained rigid glass network in the amorphous matrix is important for its thermal stability and therefore not undergoing a phase-change (crystallization) process during the threshold switching. A simple, but efficient parameter to define the matrix rigidity is the MCN of a material, which is simply derived from the chemical composition by averaging the formal coordination numbers of the atoms, weighted by their concentration in the material. A 2.4 < MCN < 3.0 is required for OTS chalcogenide glasses to be considered rigid in normal conditions [60]. Our materials are, indeed, rigid-glass-formers by the MCN criterium, which is in the range of 2.7-3.0, as listed in the Table 1. Since both MCN and #e are derived from the composition stoichiometry, the two parameters have a reciprocal relationship (see Supplementary Fig S1 and S2).

B. Threshold / first-fire voltages

Instead of discussing the dependence on the threshold/first-fire/holding electric field, which is the fundamental parameter, for the sake of convenience we will discuss in this work directly about the respective voltages. Translating between the two could be performed in a first-order approximation by division of the voltage to the films thickness (20nm). The computed mobility gaps E_μ of the investigated OTS chalcogenides show positive correlations with both first-fire V_{ff} and threshold voltage V_{th} , as shown in the Fig. 3a. For certain materials, the mobility gap error bars are rather large, which can be interpreted as limited atomic model size, but also wide local variation in the material are expected. For that matter, finding trends in a single class of materials is challenging, nevertheless, the median values for all material classes together seem to show a rather clear qualitative trend. In the same time, there is a positive correlation between experimental V_{ff} and V_{th} (Fig. 3b).

To understand these correlations, we start by building a qualitative model for OTS switching, in which we try to unify together concepts from other models: the first-fire can be interpreted as energetic generation of higher-energy (in a local minimum on the potential energy surface of the amorphous matrix) working set of OTS traps (in the valence or conduction tail-states). That is illustrated by the negative correlation of the material formation energy with the V_{th}, as illustrated in Fig. 3c (and therefore E_μ, as we already established a positive correlation between the two): the higher the material (formation) energy, the more traps in the gap are at higher energy levels, hence they would require lower electric field (V_{th}/OTS thickness) to switch ON.

Being in a higher-energy state, those traps eventually will relax back to a lower-energy local atomic coordination environment (a process called ageing) or get annealed during billions of endurance cycles of the device. This will lead to V_{th} drift towards initial V_{ff}, which usually is referred to as threshold voltage instability or relaxation [22,39,61]. A simple interpretation of the working set of traps in OTS is depicted in Fig. 4: if we expect the OTS material to switch ON at a certain electric field, the switching process involves trap states delocalization/ percolation of the material or trap energy alignment with a full-device-width-delocalized state, *i.e,* conduction/ valence state (the equivalent of the band in the crystalline phase). The energetic alignment of the traps due to the applied electric field through Stark effect [62] will increase exponentially the tunnelling probability of the charge carrier between the localized states. The other possibility is to increase atomic orbital overlap and hence delocalize the state on a larger volume in space, ultimately short-circuiting the device, therefore contributing to an increased conductivity [22].

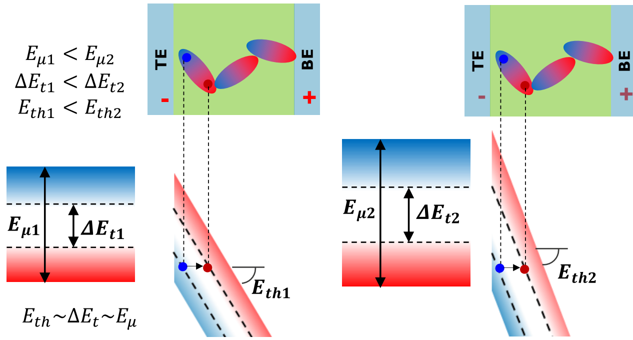

Fig. 4. Threshold field (E_{th}) dependence on mobility/trap gap: larger mobility/trap gaps require higher fields to align trap energies for optimal tunnelling/delocalization.

If we consider the traps to be conduction/ valence tail states that energetically are close to the conduction/ valence edges, then with an increase in the mobility gap E_μ, there will be an increase in trap gap ΔE_t, hence there will be necessary a higher field to align the traps to switch ON the material. One may argue that the first-fire corresponds to an initial situation, when the initially-available traps are shallower and give larger trap/mobility gaps, therefore require larger ON-switching fields. However, the DFT-extracted traps are not only in the tails, could be anywhere in the mobility gap and not necessarily OTS-active. This results in a much weaker trap gap correlation with threshold voltage (Fig. 5). Different material classes will show different capability to change the trap levels/gaps with the first-fire high-energy conditioning pulse and it shows as different slopes in the E_μ-V_{th} and E_μ-V_{ff} trends (Fig. 3a).

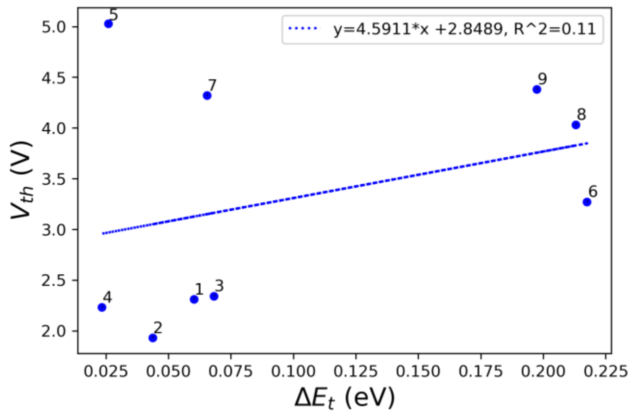

Fig. 5. Threshold voltage (V_{th}) correlation with the trap gap (ΔE_t) is positive but weak. Data points labeled with material id from Table 1.

One expects threshold switching ON to involve more of electronic state overlap/ delocalization with less atomic relaxation than in the case of the first-fire event. While in the ON state, the traps that keep the channel open are maintained in a higher-energy state and fully-occupied-with-charge-carriers (if time-averaged). Joule heating effects contribute to this high-energy state as well. On the ramp-down of the electric field while in the Ohmic regime of the OTS-ON state, at certain minimal current (hold current and voltage) the OTS will switch OFF (Fig. 1b). In the following section we investigate the correlations of the hold parameters with electronic properties.

C. Hold voltage / current

At the minimum current level (I_h), the thermal energy is probably dissipated faster than the current can sustain with Joule heating, therefore the traps relax back to the localized configuration. The traps become empty of carriers, the current flow stops, switching OFF the OTS device. In the Fig. 6a,b we correlated the the V_h and I_h with the mobility gap E_μ. The direct dependency indicates that the farther apart in energy the defects (tail states near conduction/valence edges) are, the higher power (V_h and I_h) is needed to keep them communicating with each-other,*i.e.*, at the same energy to have efficient tunnelling and orbital overlap/delocalization, hence good electrical conduction channel. The observed positive correlation indicates that holding parameters are working in the same manner as the V_{th}/ V_{ff} are: the higher the mobility gap (more insulating), the higher the electrical parameter V_{th}/ V_{ff} is. While not important for voltage-controlled devices, another important factor that might help keeping the ON-state active is light irradiation, which could be an interesting research topic for light-controlled chips or interconnects.

D. Dielectric response

In analogy with the phase-change materials, where there is a high optical contrast between high and low resistance states of the material, the same change of dielectric response is expected to occur in the ON state of the OTS. However, there is a difference: since in OTS the ON state is spanning only across few localized traps bridging the conduction and valence edges, or forming a percolation path, only a small part of the total material volume is involved in the conduction process and will change the dielectric response properties. In the phase-change devices, this type of local percolation is usually referred to as filamentation [63], which makes it challenging to measure the dielectric response change by optical means.

Theoretically, however, we can assess the change in the dielectric response of the material. More precisely, we will calculate the Born effective charges (Z^*), *i.e.*, the atom's ability to change the polarizability with atomic displacement. Seminal work by Raty et al. on the link of the Born effective charges and threshold switching was published in the connection with the metavalent bonding concept [7,40]. On the basis of the DFT-computed Z^* charges, we defined an 'OTS-gauge' parameter, that shows the capacity of the material to increase the number of atoms with an increased Z^* upon charge injection in the system. A closely-related metric has been shown to be a good characteristic of the threshold-switching materials [40]. In our set of materials, we found a strong positive correlation of the OTS-gauge with V_{ff} and V_{th} (Fig. 6c).

First-fire (V_{ff}), threshold (V_{th}), hold voltages (V_h), and hold current (I_h) are showing positive correlations with the mobility gap (E_μ) and OTS gauge (Z^*), hence all these parameters were categorized as *insulating* group since they have a direct relationship to the insulating properties of the materials. Those are high mobility gap and low leakage current, and are negatively correlating with each other, as shown in Fig. 6d.

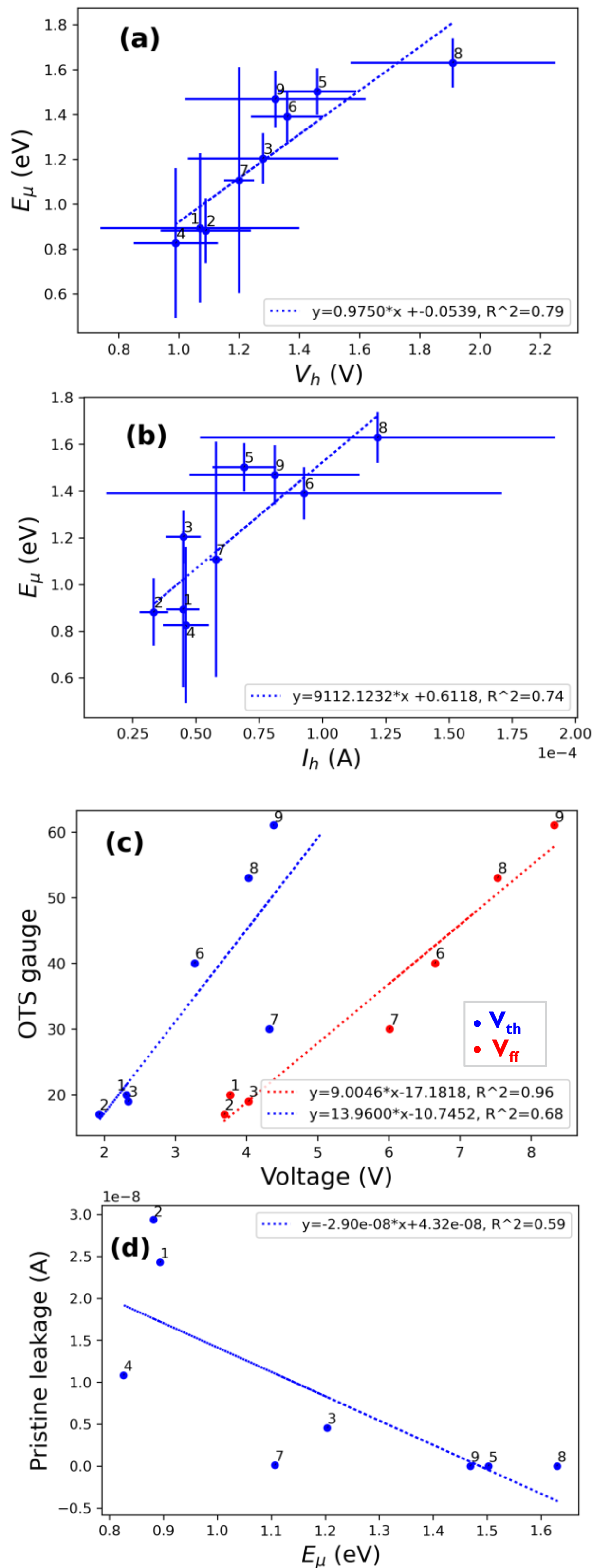

Fig. 6. a) Holding voltage (V_h) and b) current (I_h) show positive correlation with the mobility gap (E_m). c) Positive correlation of OTS gauge with V_{th} and V_{ff} d) Pristine device leakage current negatively correlates to the materials' mobility gap. Data points labeled with material id from Table 1.

E. Atomic coordination environment

In the phase-change materials (PCM) the transition from insulating phase to conductive phase is interpreted as a transition (phase-change) in the bulk of the material, from a sp^3-hybridized, Lewis-octet-rule-following insulating amorphous state, to a resonant/hyper-bonding conducting crystalline phase, as depicted in Fig. 7a. In the OTS materials, a similar atomic environment change is expected but on a very local atomic scale, as imagined in Fig. 7b. To better understand the effect of the local environment, we analyzed the local coordination around each atom and averaged over all 10 different atomic models for each composition. From Fig. 7c is clear that indeed, the tetrahedral bond angles of the amorphous OTS are correlating positively with all *insulating* parameters group and negatively correlating to the *conductive* group. For this reason, we can categorize the local tetrahedral environment as insulating that has a normal coordination with 2-4 nearest-neighbors. The over-coordinated atomic environments that have 5-7 nearest-neighbors, on the other hand, are correlating with the *conductive* group of parameters, that will be discussed in the next section. From these observations, we can conclude that the atomic environment change is most probably also happening during the threshold switching: upon charge excitation (or injection), local atomic environment changes in terms of bond alignment/orbital overlap and results in larger spatial delocalization of the state(s) in the gap because of the energetic alignment of 2 or more local states under threshold field. This in turn, results in energy (mobility gap) percolation from mid-gap (or valence) to conduction (tail-) states, or film percolation (physical space) from top to bottom electrode.

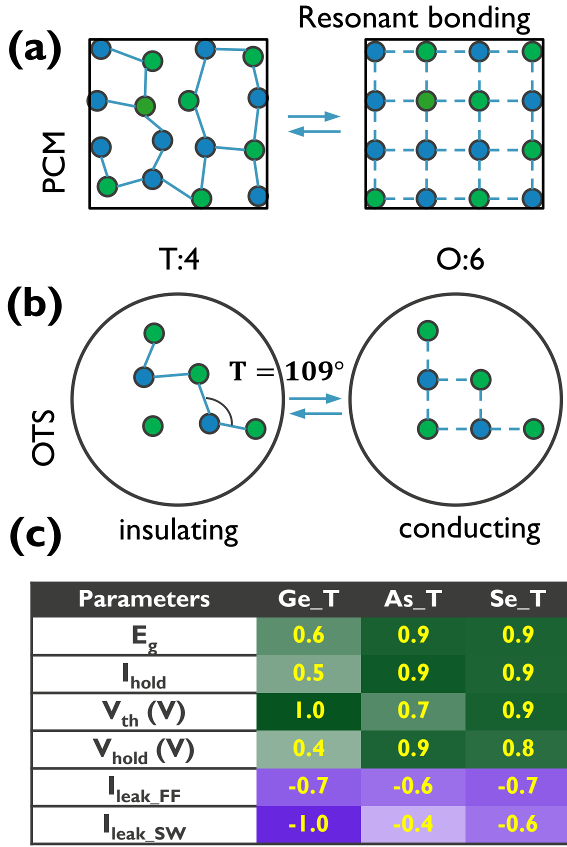

Parameters	Ge_T	As_T	Se_T
E_g	0.6	0.9	0.9
I_{hold}	0.5	0.9	0.9
V_{th} (V)	1.0	0.7	0.9
V_{hold} (V)	0.4	0.9	0.8
I_{leak_FF}	-0.7	-0.6	-0.7
I_{leak_SW}	-1.0	-0.4	-0.6

Fig. 7. a) The conduction increases in PCM upon crystallization of the bulk of material, the resonant bonding defines octahedral (O:6) /conducting local coordination b) Similar changes expected in OTS, but on a local scale c) Pearson correlation factors of the tetrahedral (T:4) local environment with insulating (green) and conductive (violet) groups of parameters.

F. Leakage and defects

By now, we established a group of parameters that can be categorized as *insulating* (Section IID). Experiment-extracted numbers for trap concentration (N_d) and the leakage current (I_{leak}), on the other hand, can be categorized as *conductive* parameters. This means they correlate positively among themselves but show a negative correlation with insulating set of parameters (see Fig. 8 and Fig. 6d).

The local coordination analysis shows that normal (tetrahedral) coordination is inversely proportional (negative correlation) to the conduction (leakage currents before first-fire I_{leak_ff} and during switching I_{leak_sw} Fig. 7c). Over-coordination, however, shows a positive correlation to the *conductive* group of parameters (leakage I_{leak} and trap concentration N_d shown in Fig. 8). That can be rationalized in terms of local coordination environment, since the aligned bonds are predominant in over-coordinated sites (with 5-7 nearest-neighbors) and the alignment of the bonds was linked to the threshold switching of the material [40].

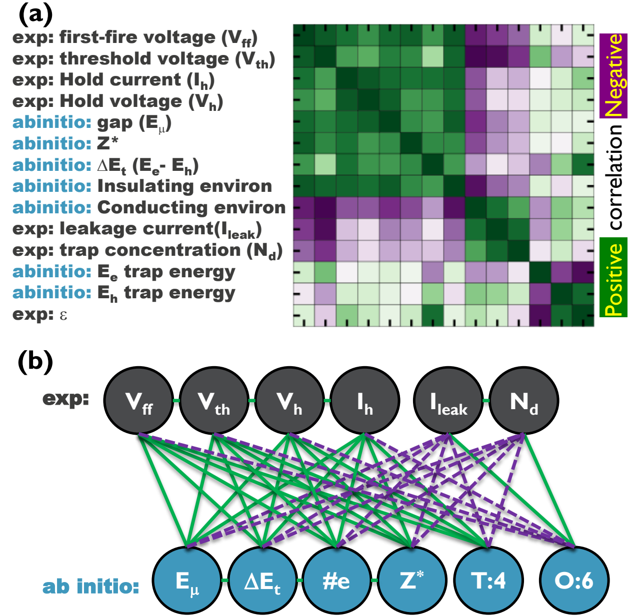

Fig. 8 a) Experimental and ab-initio parameter correlation matrix, colored by the Pearson correlation factors b) Correlation links between experimental parameters and ab-initio properties. Positive correlations are full lines, negative correlations - dashed lines.

IV. Conclusion

The goal of the study is to obtain quantitative insight into the dependence of the experimental device performance parameters (like first-fire, threshold, hold voltages or hold/ leakage currents) upon theoretically simulated material properties (like mobility gap, trap position in the gap or local atomic coordination environment). For that, we investigated a set of 9 materials with different stoichiometries/compositions from both experimental and theoretical perspectives, that contain a set of 5 elements: Si, Ge, As, Se and Te. In the approximation that parameter interdependence is relatively independent of the constituent elements and relies more on the general electronic properties of the amorphous materials, we are tempted to conclude that the found dependencies could be extrapolated outside the available set of elements, as long the electronic structure will have parameters close to the ones in the available set of materials.

The findings allow us to group the experimental and theoretical parameters into two distinct groups, named *insulating* and *conductive* groups of parameters, based on positive correlations within the group and negative correlation between the groups (see Fig. 8). More specifically, in the first *insulating* group, the experimental V_{ff}, V_{th}, V_h and I_h correlate positively with theoretical E_μ, ΔE_t, average number of valence electrons, OTS gauge (Z^*) and local atomic tetrahedral environment. For the second *conductive* group, the N_d and I_{leak}, were found to show negative correlation to the same theoretical parameters. This experiment-vs-theory calibration exercise allows us to predict first-fire, threshold and hold voltages (not to forget the film thickness correction, since the dependencies are on the electric field and not voltage) and currents of an arbitrary amorphous material composition. Also, it is possible to theoretically predict if the material will show promising OTS

behavior from first-principles simulations alone by means of OTS-gauge. Further high-throughput screening for environmentally-friendly OTS materials that accounts for these relations in selecting the threshold voltage bracket are ongoing [41].

Supporting Information

Correlation of valence electrons and mean coordination numbers with threshold and hold voltages.

Acknowledgment

This work was carried out in the framework of the imec Core CMOS – Active Memory Program. T.R. thanks FWO for funding (grant no 1SD4721).

References

(1) Wuttig, M.; Yamada, N. Phase-change materials for rewriteable data storage. *Nature Materials* **2007**, *6* (11), 824-832. https://doi.org/10.1038/nmat2009.

(2) Shportko, K.; Kremers, S.; Woda, M.; Lencer, D.; Robertson, J.; Wuttig, M. Resonant bonding in crystalline phase-change materials. *Nature Materials* **2008**, *7* (8), 653-658. https://doi.org/10.1038/nmat2226.

(3) Horie, M.; Nobukuni, N.; Kiyono, K.; Ohno, T. High speed rewritable DVD up to 20m/s with nucleation-free eutectic phase-change material of Ge(Sb70Te30)+Sb. In *Conference on Optical Data Storage (ODS2000)*, Whistler, Canada, May 14-17, 2000; Vol. 4090, pp 135-143. https://doi.org/10.1117/12.399373.

(4) Zhang, Y. F.; Chou, J. B.; Li, J. Y.; Li, H. S.; Du, Q. Y.; Yadav, A.; Zhou, S.; Shalaginov, M. Y.; Fang, Z. R.; Zhong, H. K.; Roberts, C.; Robinson, P.; Bohlin, B.; Rios, C.; Lin, H. T.; Kang, M.; Gu, T.; Warner, J.; Liberman, V.; Richardson, K.; Hu, J. J. Broadband transparent optical phase change materials for high-performance nonvolatile photonics. *Nature Communications* **2019**, *10,* 4279. https://doi.org/10.1038/s41467-019-12196-4.

(5) Zhu, M.; Ren, K.; Song, Z. T. Ovonic threshold switching selectors for three-dimensional stackable phase-change memory. *Mrs Bulletin* **2019**, *44* (9), 715-720. https://doi.org/10.1557/mrs.2019.206.

(6) Xu, M.; Miao, X. S. Deep machine learning unravels the structural origin of mid-gap states in chalcogenide glass for high-density memory integration. *Infomat* **2022**, *4*, e12315. https://doi.org/10.1002/inf2.12315.

(7) Noe, P.; Verdy, A.; d'Acapito, F.; Dory, J. B.; Bernard, M.; Navarro, G.; Jager, J. B.; Gaudin, J.; Raty, J. Y. Toward ultimate nonvolatile resistive memories: The mechanism behind ovonic threshold switching revealed. *Science Advances* **2020**, *6* (9), eaay2830. https://doi.org/10.1126/sciadv.aay2830.

(8) Loke, D. K.; Skelton, J. M.; Lee, T. H.; Zhao, R.; Chong, T. C.; Elliott, S. R. Ultrafast Nanoscale Phase-Change Memory Enabled By Single-Pulse Conditioning. *Acs Applied Materials & Interfaces* **2018**, 10, 41855-41860. https://doi.org/10.1021/acsami.8b16033.

(9) Go, S. X.; Lee, T. H.; Elliott, S. R.; Bajalovic, N.; Loke, D. K. A fast, low-energy multi-state phase-change artificial synapse based on uniform partial-state transitions. *Apl Materials* **2021**, 9, 091103. https://doi.org/10.1063/5.0056656.

(10) Sun, L.; Zhou, Y. X.; Wang, X. D.; Chen, Y. H.; Deringer, V. L.; Mazzarello, R.; Zhang, W. Ab initio molecular dynamics and materials design for embedded phase-change memory. *Npj Computational Materials* **2021**, *7* (1), 29. https://doi.org/10.1038/s41524-021-00496-7.

(11) Xu, Y. Z.; Wang, X. D.; Zhang, W.; Schafer, L.; Reindl, J.; vom Bruch, F.; Zhou, Y. X.; Evang, V.; Wang, J. J.; Deringer, V. L.; Ma, E.; Wuttig, M.; Mazzarello, R. Materials Screening for Disorder-Controlled Chalcogenide Crystals for Phase-Change Memory Applications. *Advanced Materials* **2021**, *33* (9), 2006221. https://doi.org/10.1002/adma.202006221.

(12) Ding, K. Y.; Wang, J. J.; Zhou, Y. X.; Tian, H.; Lu, L.; Mazzarello, R.; Jia, C. L.; Zhang, W.; Rao, F.; Ma, E. Phase-change heterostructure enables ultralow noise and drift for memory operation. *Science* **2019**, *366* (6462), 210-215. https://doi.org/10.1126/science.aay0291.

(13) Bez, R.; Camerlenghi, E.; Modelli, A.; Visconti, A. Introduction to Flash memory. *Proceedings of the Ieee* **2003**, *91* (4), 489-502. https://doi.org/10.1109/jproc.2003.811702.

(14) Chung, A.; Deen, J.; Lee, J. S.; Meyyappan, M. Nanoscale memory devices. *Nanotechnology* **2010**, *21* (41), 412001. https://doi.org/10.1088/0957-4484/21/41/412001.

(15) Takeuchi, K.; Hatanaka, T.; Tanakamaru, S. Highly reliable, high speed and low power NAND flash memory-based Solid State Drives (SSDs). *Ieice Electronics Express* **2012**, *9* (8), 779-794. https://doi.org/10.1587/elex.9.779.

(16) Burr, G. W.; Kurdi, B. N.; Scott, J. C.; Lam, C. H.; Gopalakrishnan, K.; Shenoy, R. S. Overview of candidate device technologies for storage-class memory. *Ibm Journal of Research and Development* **2008**, *52* (4-5), 449-464. https://doi.org/10.1147/rd.524.0449.

(17) Baek, S.; Choi, J.; Lee, D.; Noh, S. H. Energy-Efficient and High-Performance Software Architecture for Storage Class Memory. *Acm Transactions on Embedded Computing Systems* **2013**, *12* (3), 81. https://doi.org/10.1145/2442116.2442131.

(18) Yang, J. J.; Strukov, D. B.; Stewart, D. R. Memristive devices for computing. *Nature Nanotechnology* **2013**, *8* (1), 13-24. https://doi.org/10.1038/nnano.2012.240.

(19) Li, Y. B.; Wang, Z. R.; Midya, R.; Xia, Q. F.; Yang, J. J. Review of memristor devices in neuromorphic computing: materials sciences and device challenges. *Journal of Physics D-Applied Physics* **2018**, *51* (50), 503002. https://doi.org/10.1088/1361-6463/aade3f.

(20) Burr, G. W.; Shenoy, R. S.; Virwani, K.; Narayanan, P.; Padilla, A.; Kurdi, B.; Hwang, H. Access devices for 3D crosspoint memory. *Journal of Vacuum Science & Technology B* **2014**, *32* (4), 040802. https://doi.org/10.1116/1.4889999.

(21) Govoreanu, B.; Donadio, G. L.; Opsomer, K.; Devulder, W.; Afanasiev, V.; Witters, T.; Clima, S.; Avasarala, N. S.; Redolfi, A.; Kundu, S.; Richard,O.; Tsvetanova,D.; Pourtois,G.; Detavernier,C.; Goux,L; Kar, G.S. Thermally stable integrated Se-based OTS selectors with >20 MA/cm2 current drive,>3.103 half-bias nonlinearity, tunable threshold voltage and excellent endurance. In *2017 Symposium on VLSI Technology*, 2017; pp T92-T93. https://doi.org/10.23919/VLSIT.2017.7998207.

(22) Clima, S.; Govoreanu, B.; Opsomer, K.; Velea, A.; Avasarala, N. S.; Devulder, W.; Shlyakhov, I.; Donadio, G. L.; Witters, T.; Kundu, S.; Goux,L.; Afanasiev,V.; Kar,G.S.; Pourtois,G. Atomistic investigation of the electronic structure, thermal properties and conduction defects in Ge-rich GeSe materials for selector applications. In *2017 IEEE International Electron Devices Meeting (IEDM)*, 2017; pp 4.1.1-4.1.4. https://doi.org/10.1109/IEDM.2017.8268323.

(23) Ovshinsky, S. R. Reversible Electrical Switching Phenomena in Disordered Structures. *Physical Review Letters* **1968**, *21* (20), 1450-1453.

(24) Chekol, S. A.; Yoo, J.; Park, J.; Song, J.; Sung, C.; Hwang, H. A C-Te-based binary OTS device exhibiting excellent performance and high thermal stability for selector application. *Nanotechnology* **2018**, *29* (34), 345202. https://doi.org/10.1088/1361-6528/aac9f5.

(25) Ravsher, T.; Garbin, D.; Fantini, A.; Degraeve, R.; Clima, S.; Donadio, G.; Kundu, S.; Hody, H.; Devulder, W.; Van Houdt, J.; Afanas'ev, V.; Delhougne, R.; Kar, G. Enhanced performance and low-power capability of SiGeAsSe-GeSbTe 1S1R phase-change memory operated in bipolar mode. In *2022 IEEE Symposium on VLSI Technology and Circuits (VLSI Technology and Circuits)*, 12-17 June 2022; pp 312-313. https://doi.org/10.1109/ VLSITechnologyandCir46769.2022.9830199.

(26) Jia, S. J.; Li, H. L.; Gotoh, T.; Longeaud, C.; Zhang, B.; Lyu, J.; Lv, S. L.; Zhu, M.; Song, Z. T.; Liu, Q.; Robertson, J.; Liu, M. Ultrahigh drive current and large selectivity in GeS selector. *Nature Communications* **2020**, *11* (1), 4636. https://doi.org/10.1038/s41467-020-18382-z.

(27) Gu, R. C.; Xu, M.; Yu, R.; Qiao, C.; Wang, C. Z.; Ho, K. M.; Wang, S. Y.; Miao, X. S. Structural features of chalcogenide glass SiTe: An ovonic threshold switching material. *Apl Materials* **2021**, *9* (8), 081101. https://doi.org/10.1063/5.0059845.

(28) Gu, R. C.; Xu, M.; Qiao, C.; Wang, C. Z.; Ho, K. M.; Wang, S. Y.; Miao, X. S. How arsenic makes amorphous GeSe a robust chalcogenide glass for advanced memory integration. *Scripta Materialia* **2022**, *218*, 114834. https://doi.org/10.1016/j.scriptamat.2022.114834.

(29) Pruss-Ustun, A.; Vickers, C.; Haefliger, P.; Bertollini, R. Knowns and unknowns on burden of disease due to chemicals: a systematic review. *Environmental Health* **2011**, *10*, 9. https://doi.org/10.1186/1476-069X-10-9.

(30) Fulcher, K.; Herman, G. Setting the Research Agenda on the Health Effects of Chemicals. *International Journal of Environmental Research and Public Health* **2014**, *11* (1), 1049-1057. https://doi.org/10.3390/ijerph110101049.

(31) Adler, D.; Shur, M. S.; Silver, M.; Ovshinsky, S. R. THRESHOLD SWITCHING IN CHALCOGENIDE-GLASS THIN-FILMS. *Journal of Applied Physics* **1980**, *51* (6), 3289-3309, Article. https://doi.org/10.1063/1.328036.
(32) Pirovano, A.; Lacaita, A. L.; Benvenuti, A.; Pellizzer, F.; Bez, R. Electronic switching in phase-change memories. *Ieee Transactions on Electron Devices* **2004**, *51* (3), 452-459. https://doi.org/10.1109/ted.2003.823243.
(33) Pirovano, A.; Lacaita, A. L.; Pellizzer, F.; Kostylev, S. A.; Benvenuti, A.; Bez, R. Low-field amorphous state resistance and threshold voltage drift in chalcogenide materials. *Ieee Transactions on Electron Devices* **2004**, *51* (5), 714-719. https://doi.org/10.1109/ted.2004.825805.
(34) Ielmini, D.; Zhang, Y. G. Analytical model for subthreshold conduction and threshold switching in chalcogenide-based memory devices. *Journal of Applied Physics* **2007**, *102* (5), 054517. https://doi.org/10.1063/1.2773688.
(35) Karpov, V. G.; Kryukov, Y. A.; Savransky, S. D.; Karpov, I. V. Nucleation switching in phase change memory. *Applied Physics Letters* **2007**, *90* (12), 3, https://doi.org/10.1063/1.2715024.
(36) Karpov, V. G.; Kryukov, Y. A.; Karpov, I. V.; Mitra, M. Field-induced nucleation in phase change memory. *Physical Review B* **2008**, *78* (5), 052201, https://doi.org/10.1103/PhysRevB.78.052201.
(37) Le Gallo, M.; Athmanathan, A.; Krebs, D.; Sebastian, A. Evidence for thermally assisted threshold switching behavior in nanoscale phase-change memory cells. *Journal of Applied Physics* **2016**, *119* (2), 025704. https://doi.org/10.1063/1.4938532.
(38) Clima, S.; Garbin, D.; Devulder, W.; Keukelier, J.; Opsomer, K.; Goux, L.; Kar, G. S.; Pourtois, G. Material relaxation in chalcogenide OTS SELECTOR materials. *Microelectronic Engineering* **2019**, *215*, 110996. https://doi.org/10.1016/j.mee.2019.110996.
(39) Clima, S.; Garbin, D.; Opsomer, K.; Avasarala, N. S.; Devulder, W.; Shlyakhov, I.; Keukelier, J.; Donadio, G. L.; Witters, T.; Kundu, S.; Govoreanu, B.; Goux, L.; Detavernier, C.; Afanas'ev, V.; Kar, G. S.; Pourtois, G. Ovonic Threshold-Switching Ge_xSe_y Chalcogenide Materials: Stoichiometry, Trap Nature, and Material Relaxation from First Principles. *Physica Status Solidi-Rapid Research Letters* **2020**, *14* (5), 1900672. https://doi.org/10.1002/pssr.201900672.
(40) Raty, J. Y.; Noe, P. Ovonic Threshold Switching in Se-Rich GexSe1-x Glasses from an Atomistic Point of View: The Crucial Role of the Metavalent Bonding Mechanism. *Physica Status Solidi-Rapid Research Letters* **2020**, *14* (5), 1900581. https://doi.org/10.1002/pssr.201900581.
(41) Matsubayashi, D.; Clima, S.; Ravsher, T.; Garbin, D.; Delhougne, R.; Kar, G. S.; Pourtois, G. OTS Physics-based Screening for Environment-friendly Selector Materials. In *2022 IEEE International Electron Devices Meeting (IEDM)*, 2022.
(42) Hutter, J.; Iannuzzi, M.; Schiffmann, F.; VandeVondele, J. cp2k: atomistic simulations of condensed matter systems. *Wiley Interdisciplinary Reviews: Computational Molecular Science* **2014**, *4* (1), 15-25. https://doi.org/10.1002/wcms.1159.
(43) Goedecker, S.; Teter, M.; Hutter, J. Separable dual-space Gaussian pseudopotentials. *Physical Review B* **1996**, *54* (3), 1703-1710. https://doi.org/10.1103/PhysRevB.54.1703.
(44) Perdew, J. P.; Burke, K.; Ernzerhof, M. Generalized gradient approximation made simple. *Physical Review Letters* **1996**, *77* (18), 3865-3868. https://doi.org/10.1103/PhysRevLett.77.3865.
(45) Heyd, J.; Scuseria, G. E. Assessment and validation of a screened Coulomb hybrid density functional. *Journal of Chemical Physics* **2004**, *120* (16), 7274-7280. https://doi.org/10.1063/1.1668634.
(46) Youn, Y.; Kang, Y.; Han, S. An efficient method to generate amorphous structures based on local geometry. *Computational Materials Science* **2014**, *95*, 256-262. https://doi.org/10.1016/j.commatsci.2014.07.053.
(47) de Jamblinne de Meux, A.; Pourtois, G.; Genoe, J.; Heremans, P. Effects of hole self-trapping by polarons on transport and negative bias illumination stress in amorphous-IGZO. *Journal of Applied Physics* **2018**, *123* (16), 161513. https://doi.org/10.1063/1.4986180.
(48) Guidon, M.; Hutter, J.; VandeVondele, J. Auxiliary Density Matrix Methods for Hartree−Fock Exchange Calculations. *Journal of Chemical Theory and Computation* **2010**, *6* (8), 2348-2364. https://doi.org/10.1021/ct1002225.
(49) Murphy, N. C.; Wortis, R.; Atkinson, W. A. Generalized inverse participation ratio as a possible measure of localization for interacting systems. *Physical Review B* **2011**, *83* (18), 184206. https://doi.org/10.1103/PhysRevB.83.184206.
(50) Devulder, W.; Garbin, D.; Clima, S.; Donadio, G. L.; Fantini, A.; Govoreanu, B.; Detavernier, C.; Chen, L.; Miller, M.; Goux, L.; Van Elshocht, S.; Swerts, J.; Delhougne, R.; Kar, G. S. A combinatorial study of SiGeAsTe thin films for application as an Ovonic threshold switch selector. *Thin Solid Films* **2022**, *753*, 139278. https://doi.org/10.1016/j.tsf.2022.139278.
(51) Degraeve, R.; Ravsher, T.; Kabuyanagi, S.; Fantini, A.; Clima, S.; Garbin, D.; Kar, G. S.; Ieee. Modeling and spectroscopy of ovonic threshold switching defects. In *IEEE International Reliability Physics Symposium (IRPS)*, Mar 21-24, 2021; pp 1-5. https://doi.org/10.1109/irps46558.2021.9405114.
(52) Ghosez, P.; Michenaud, J. P.; Gonze, X. Dynamical atomic charges: The case of ABO(3) compounds. *Physical Review B* **1998**, *58* (10), 6224-6240. https://doi.org/10.1103/physrevb.58.6224.
(53) Waroquiers, D.; Gonze, X.; Rignanese, G. M.; Welker-Nieuwoudt, C.; Rosowski, F.; Gobel, M.; Schenk, S.; Degelmann, P.; Andre, R.; Glaum, R.; Hautier, G. Statistical Analysis of Coordination Environments in Oxides. *Chemistry of Materials* **2017**, *29* (19), 8346-8360. https://doi.org/10.1021/acs.chemmater.7b02766.
(54) Waroquiers, D.; George, J.; Horton, M.; Schenk, S.; Persson, K. A.; Rignanese, G. M.; Gonze, X.; Hautier, G. ChemEnv: a fast and robust coordination environment identification tool. *Acta Crystallographica Section B-Structural Science Crystal Engineering and Materials* **2020**, *76*, 683-695. https://doi.org/10.1107/s2052520620007994.
(55) Li, H. L.; Robertson, J. Materials Selection and Mechanism of Non-linear Conduction in Chalcogenide Selector Devices. *Scientific Reports* **2019**, *9*, 1867. https://doi.org/10.1038/s41598-018-37717-x.
(56) Luo, M. B.; Wuttig, M. The dependence of crystal structure of Te-based phase-change materials on the number of valence electrons. *Advanced Materials* **2004**, *16* (5), 439. https://doi.org/10.1002/adma.200306077.
(57) Velea, A.; Opsomer, K.; Devulder, W.; Dumortier, J.; Fan, J.; Detavernier, C.; Jurczak, M.; Govoreanu, B. Te-based chalcogenide materials for selector applications. *Scientific Reports* **2017**, *7*, 8103. https://doi.org/10.1038/s41598-017-08251-z.
(58) Abrahams, E.; Anderson, P. W.; Licciardello, D. C.; Ramakrishnan, T. V. Scaling Theory of Localization: Absence of Quantum Diffusion in Two Dimensions. *Physical Review Letters* **1979**, *42* (10), 673-676. https://doi.org/10.1103/PhysRevLett.42.673.
(59) Anderson, P. W. Absence of Diffusion in Certain Random Lattices. *Physical Review* **1958**, *109* (5), 1492.
(60) Read, J. C.; Stewart, D. A.; Reiner, J. W.; Terris, B. D. Evaluating Ovonic Threshold Switching Materials with Topological Constraint Theory. *Acs Applied Materials & Interfaces* **2021**, *13* (31), 37388-37401. https://doi.org/10.1021/acsami.1c10131.
(61) Yamaguchi, M.; Degraeve, R.; Garbin, D.; Clima, S.; Ravsher, T.; Matsubayashi, D.; Tsukamoto, T.; Delhougne, R.; Goux, L.; Kar, G. S. Understanding the Cycling-Dependent Threshold Voltage Instability in OTS Devices In *2022 IEEE International Electron Devices Meeting (IEDM)*, 2022.
(62) Epstein, P. S. The Stark Effect from the Point of View of Schroedinger's Quantum Theory. *Physical Review* **1926**, *28*, 695–710.
(63) Wuttig, M.; Bhaskaran, H.; Taubner, T. Phase-change materials for non-volatile photonic applications. *Nature Photonics* **2017**, *11* (8), 465-476. https://doi.org/10.1038/nphoton.2017.126.

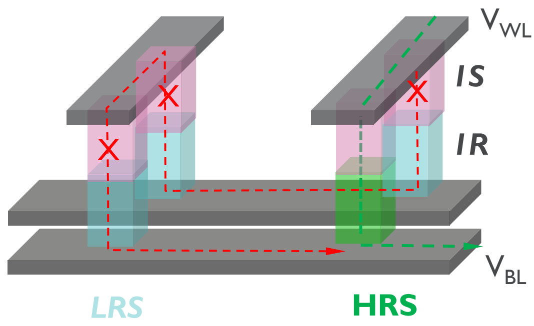
VWL
IS
IR
VBL
LRS
HRS

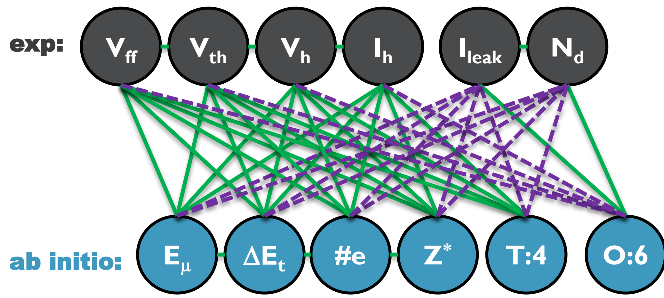
exp:
Vff
Vth
Vh
Ih
Ileak
Nd
ab initio:
Eμ
ΔEt
#e
Z*
T:4
O:6